*American Mineralogist, Volume 84, pages 1256–1269, 1999*

# Trace element distribution among rock-forming minerals in Black Hills migmatites, South Dakota: A case for solid-state equilibrium

**PETER I. NABELEK**

Department of Geological Sciences, University of Missouri-Columbia, Columbia, Missouri 65211, U.S.A.

## ABSTRACT

Proterozoic migmatites in the Black Hills, South Dakota, were examined to determine if partitioning of trace elements hosted by rock-forming minerals between melanosomes and leucosomes preserves residue-melt equilibrium that was presumably established during partial melting of pelitic lithologies. Granitic leucosomes in the Black Hills, as is often the case elsewhere, have positive Eu anomalies, are highly enriched in Sr and Ba, and are depleted in Rb and Cs relative to granites derived by partial melting of metapelites. Distributions of these trace elements between melanosomes and leucosomes cannot be simulated using mineral-melt distribution coefficients. A metamorphic reaction-progress method is used to demonstrate that the distributions approach mineral-mineral equilibrium rather than mineral-melt equilibrium. Application of published diffusion data for the relevant elements in feldspars shows that solid-state equilibrium is unlikely to have been established during subsolidus cooling. Instead, it is suggested that partial melts maintained chemical equilibrium with melanosomes during crystallization that lead to the migmatites.

## INTRODUCTION

Migmatites are of interest to petrologists because many are thought to represent source regions for granitic melts. Careful analyses of migmatites potentially can yield important information about melt-forming reactions, melt-extraction processes, and scales of chemical equilibrium in granite source regions. This study was undertaken to evaluate whether distributions of trace elements controlled by rock-forming minerals in melanosomes and leucosomes of migmatites can be used as an analogue for equilibrium between residue and melt in granite source regions. Residue-melt equilibrium is a fundamental assumption in trace element models for granite petrogenesis (Hanson 1978). Previous studies of peraluminous migmatites have demonstrated that high field-strength elements, such as Zr, Th, and trivalent rare-earth elements (REE), may not reach equilibrium concentrations in partial melts because their concentrations are controlled by accessory minerals that may be refractory or remain as inclusions in residual major minerals during melting (Bea 1996; Johannes et al. 1995; Nabelek and Glascock 1995; Sawyer 1991; Watt and Harley 1993; Watt et al. 1996). Observations of depletions in high field-strength elements have led to inferences of rapid melt extraction or rapid cooling of granite source regions (e.g., Sawyer 1991; Watt et al. 1996).

In contrast to high field-strength elements, in many cases the behavior of $Eu^{2+}$, Rb, Cs, Sr, and Ba in migmatites is different. Although in some leucosomes Sr and Ba occur in relatively low concentrations and REE patterns have negative Eu anomalies, in many other leucosomes these elements are highly enriched in comparison to spatially related leucogranites (e.g., Brown and D'Lemos 1991; Power 1993). Such enrichments in the divalent cations previously have been attributed to processes such as fractional crystallization of feldspars in leucosomes or preferential melting of feldspar-containing layers (Cuney and Barbey 1982; Sawyer 1987; Johannes et al. 1995). However, Fourcade et al. (1992) argued that trace element distributions between melanosomes and leucosomes in St. Malo, France, migmatites approach mineral-mineral equilibrium rather than residue-melt equilibrium. They ascribed this to reequilibration of trace elements among melanosome and leucosome minerals by diffusion during cooling of the migmatite terrane. Using published diffusion rates of trace elements in relevant minerals, Fourcade et al. (1992) inferred the cooling rate of the St. Malo migmatite terrane. In contrast, Bea et al. (1994) assumed that the distribution of alkali, alkali earth, transition metals, and some other non-high field-strength elements between melanosome minerals and leucosomes in Peña Negra, Spain, migmatites represents mineral-melt equilibrium. One result of this assumption is that many of their inferred mineral/melt distribution coefficients are drastically different from those predicted by experimental studies and observed in rhyolite systems (cf. Icenhower and London 1995, 1996; Mahood and Hildreth 1983; Nash and Crecraft 1985). This raises the question of whether the distribution coefficients of Bea et al. (1994) in fact reflect frozen residue-melt equilibrium rather than mineral-mineral equilibrium.

The purpose of this paper is to evaluate the distributions of period-four transition metals, Eu, Rb, Cs, Sr, and Ba in Black Hills, South Dakota, migmatites because these elements are critical to petrogenetic models for magma-forming processes in the crust. The commonly made assumption that trace ele-

*E-mail: nabelekp@missouri.edu

ment distribution between melanosomes and leucosomes in anatectic migmatites represents residue-melt equilibrium is examined critically from the viewpoint of mineral-melt equilibrium and by a mineral reaction-progress approach, which assumes mineral-mineral equilibrium. This work builds on previous studies of the Black Hills migmatites that addressed the occurrence of partial melting (Shearer et al. 1987), the role of accessory minerals in controlling the distribution of REE in leucogranites (Nabelek and Glascock 1995), and the origin of quartz-sillimanite leucosomes in the migmatites (Nabelek 1997). The migmatites are particularly well suited for examination of trace-element distributions because the mineralogy and geochemistry of equivalent schists at lower grades are known and compositions of leucosomes can be compared with the neighboring Harney Peak leucogranite, which was derived by partial melting of rocks equivalent to the migmatite protoliths. Thus, the geologic context of the migmatites places important constraints on interpretation of their chemistry.

## GEOLOGY AND METAMORPHISM OF SOUTHERN BLACK HILLS

Migmatites in the southern Black Hills are a by-product of a complex Precambrian tectonic, metamorphic, and plutonic history of rocks that became exposed during the Laramide orogeny (Redden et al. 1990). The Precambrian terrain is dominated by Late-Archean to Middle-Proterozoic quartzites and schists, including metapelites and metagraywackes, which were intruded by the Harney Peak leucogranite (HPG) and associated pegmatites (Fig. 1). In the portion of the Black Hills shown, metamorphic grade increases from garnet + chlorite to second sillimanite west of the main HPG pluton. Assemblages in the schists above the staurolite isograd include staurolite, garnet, biotite, muscovite, quartz, plagioclase, and accessory minerals, including monazite, zircon, apatite, xenotime, and graphite. The first sillimanite isograd appears to be related to the breakdown of staurolite. The second sillimanite isograd to the west and within the main HPG pluton corresponds to extensive migmatization of the schists (Shearer et al. 1987; Nabelek 1997). The migmatites are subject of this paper.

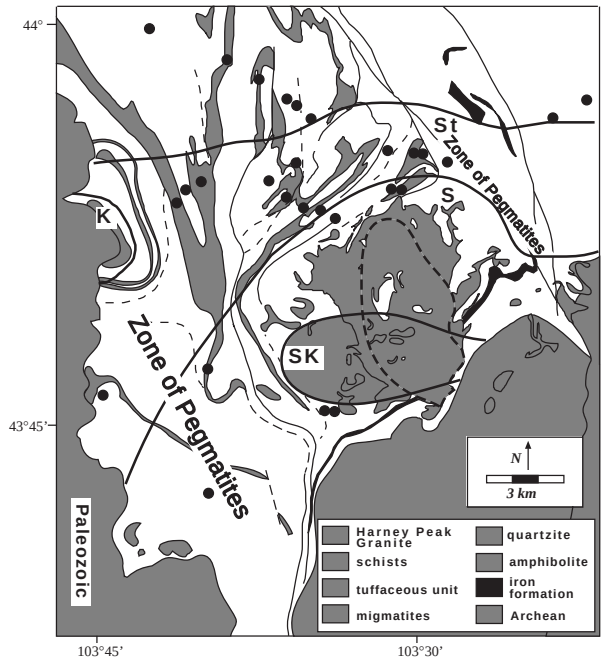


**FIGURE 1.** Geologic map of the Proterozoic terrane in the southern Black Hills (after Dewitt et al. 1989). Thin lines, including dashed lines, are faults; heavy lines are isograds. Other abbreviations: St = staurolite, S = first sillimanite, SK = second sillimanite, K = kyanite. A tuffaceous shale unit (now schist) is highlighted to show the major fold structures. Black dots show locations of chemically analyzed schist samples. Migmatites occur above second sillimanite isograd.

The dominant structural feature of schists in the southern Black Hills is a north-northwest-trending, steeply dipping foliation. However, closer to the main body of the HPG, the foliation changes from steeply dipping to flat lying and the contact between the schist and granite is mostly concordant to foliation. Within the second sillimanite zone, boudinage structures are common (Fig. 2), which implies probable intrusion of granite below the schist outcrops.

The HPG, its satellite plutons, and pegmatites were emplaced as thousands of dikes and sills. Their dominant minerals are albitic plagioclase, microcline, quartz, muscovite, and tourmaline or biotite. The granites comprise two suites with distinct $\delta^{18}O$ values and initial ratios of $^{143}Nd/^{144}Nd$ and $^{207}Pb/^{204}Pb$. Whole-rock $\delta^{18}O$ values of granites from central parts of the main pluton are 10.8–12.8‰ with an average of 12.0‰ (low-$\delta^{18}O$ suite), whereas values of samples from the flanks of the main pluton and satellite intrusions are 12.3–13.6‰ with an average of 13.1‰ (high-$\delta^{18}O$ suite; Nabelek et al. 1992b). The average of the latter values is virtually the same as the average for the country rock schists (Nabelek and Bartlett 1998). Similarly, potassium feldspars from samples of the high- and low-$\delta^{18}O$ suites define distinct $^{207}Pb/^{204}Pb$-$^{206}Pb/^{204}Pb$ arrays, with values for the high-$\delta^{18}O$ granites similar to the schists at the time of granite generation (Krogstad et al. 1993). Krogstad and Walker (1996) obtained a range of $\varepsilon_{Nd}$(1715 Ma) from –6.4 to –9.9 for the low-$\delta^{18}O$ suite and –2.0 to –7.4 for the high-$\delta^{18}O$ suite. Again, the high end of the range for the high-$\delta^{18}O$ suite overlaps that of the Proterozoic country rocks. Thus, the three isotopic systems suggest that the metasedimentary rocks are equivalent to sources of the high-$\delta^{18}O$ granite suite. Furthermore, petrogenetic models for the HPG indicate that the suite was generated mostly by muscovite dehydration-melting (Nabelek et al. 1992a; Nabelek and Bartlett 1998) as have the migmatites (see below). Because muscovite dehydration-melting is essentially a discontinuous reaction (Patiño-Douce and Harris 1998), composition of the high-$\delta^{18}O$ HPG suite serves as a useful indicator of the expected composition of leucosomes derived by partial melting of metapelitic rocks.

Ages of garnets from the metamorphic rocks range from 1760–1720 Ma, reflecting the duration of regional metamorphism (Dahl and Frei 1998; Dahl et al. 1998). Redden et al. (1990) obtained a discordant U-Pb zircon age of 1728 Ma and a concordant 1715 Ma monazite age for the HPG. The metamorphism, deformation, and granite generation are related to the Trans-Hudson orogeny (Nabelek et al. 1999).

## ANALYTICAL TECHNIQUES AND MINERAL MODES

Thirty samples of schists, seven sets of leucosome, melanosome, and mesosome, eight additional leucosomes, two melanosomes, and thirteen mesosomes were analyzed for major and trace elements (Tables 1 and 2[1]). Major elements and Sr, Ba, Pb, Ni, V, Nb, Zr, Y, and Ga were determined by X-ray fluorescence methods at Washington University, St. Louis. Rb, Cs, Th, U, Sc, Co, Cr, Zn, Ta, Hf, and REE were determined by instrumental neutron activation analysis at the University of Missouri Research Reactor. Mineral analyses were obtained on a JEOL 733 Superprobe at Washington University.

For purposes of models that are described below, it was useful to determine mineral modes in the analyzed rocks. The modes were determined by least-squares fit of mineral compositions to major element whole-rock compositions. It was assumed that

$$B_i = \sum_{j=1}^{k} A_j X_{i,j} \quad (1)$$

where $B_i$ is the weight percent of $i$th oxide in a rock consisting of $k$ minerals, $X_{i,j}$ is the weight percent of each oxide $i$ in each mineral $j$, and $A_j$ is the modal abundance of each mineral. Equation 1 was then solved by the method of least squares for $A_j$ values in each sample. Average biotite, muscovite, and garnet compositions (Table 3) and separate albite and anorthite components were used. Because the main concern for the migmatites is the mineralogy they would have had just prior to melting, only quartz, biotite, muscovite, garnet, and plagioclase were calculated for the schists (Appendix Table 1). Sillimanite is minor and therefore was not included. For the migmatites, potassium feldspar was used instead of muscovite, stoichiometric sillimanite was included, and garnet was excluded because it is lacking in most migmatites (Appendix Table 1). All calculations were done on an anhydrous basis.

## MIGMATITES

### Morphology and mineralogy

The stromatic migmatites above the second sillimanite isograd were first described by Shearer et al. (1987) who modeled the generation of granitic leucosomes assuming partial melting. Nabelek (1997) discussed the origin of quartz-sillimanite leucosomes that occur in addition to normal granitic leucosomes. In addition to leucosomes, the migmatites include well-developed dark selvages (melanosomes), and apparently non-migmatized portions (mesosomes; Fig. 2). Many leucosomes are dominated by large quartz crystals with fibrolitic sillimanite concentrated in centers of leucosomes (Fig. 2c). Tourmaline and fluorapatite are also present in some cases. Other leucosomes have normal granitic mineralogy in that they contain microcline and albite instead of sillimanite. However, all leucosomes have virtually the same $SiO_2/Al_2O_3$ ratios as the HPG (Fig. 3). The relative proportion of feldspar to sillimanite is related only to the concentration of $Na_2O + K_2O$. Leucosomes that contain feldspar are dominant in boudin necks or fractures connecting boudin necks, whereas sillimanite-containing leucosomes tend to occur in thick portions of boudins where they can be continuous for several decimeters to meters (Figs. 2a and 2b). Both feldspar-rich and sillimanite-rich leucosomes in the boudins range from about a centimeter to decimeter, whereas those in boudin necks can be decimeters across. Similar leucosome-filled boudin necks are relatively common elsewhere in anatectic migmatites (Brown 1994). They occur due to movement of melt into low pressure zones. The melanosomes are dominated by biotite and sillimanite (Fig. 2b and Fig. 4), but minor quartz also occurs in some. Biotite is generally coarser in melanosomes than in mesosomes or schists at lower grades. It also includes monazite grains that contain the majority of Th and REE in the rocks (Nabelek and Glascock 1995). Mesosomes contain various proportions of quartz, biotite, sillimanite, and plagioclase. Some mesosomes also contain poikiloblastic potassium feldspar that includes the other mesosome minerals (Fig. 2d). Included biotite in many cases preserves the dominant foliation direction of the mesosome. As expected for conditions above the second-sillimanite isograd, muscovite is lacking in the migmatites except for retrograde grains after sillimanite. The muscovite is clearly late as it has grown randomly, commonly across foliation. Similarly, anhedral tourmaline replacements of sillimanite can be found.

Based on mass-balance relationships among the leucosomes, melanosomes, mesosomes, and schists, and considerations of morphology of both leucosome types, Nabelek (1997) argued that both leucosome types were originally granitic melts that formed by partial melting of the metapelites. In addition to mass-balance arguments and occurrence of leucosomes in boudin necks, the narrow range of $SiO_2/Al_2O_3$ ratios supports partial melting rather than solid-state segregation or metasomatic processes as these would likely lead to variable ratios. Crystallization of sillimanite instead of feldspar in the partial melts is ascribed to high $H^+/(K^+ + Na^+)$ conditions resulting from the high concentration of F that is indicated by the presence of fluorapatite. K and Na were carried from the partial melts, prob-

**TABLE 3.** Mineral compositions* used in calculation of petrogenetic grid and mineral modes

| | Migmatite 124-1† | | | Average metasedimentary rocks‡ | | |
|---|---|---|---|---|---|---|
| | Biotite | Muscovite | Garnet | Biotite | Muscovite | Apatite |
| $SiO_2$ | 34.2 | 44.3 | 36.6 | 34.2 | 44.9 | 0.0 |
| $TiO_2$ | 1.91 | 0.52 | 0.03 | 1.91 | 0.48 | 0.0 |
| $Al_2O_3$ | 20.9 | 35.8 | 22.5 | 20.9 | 38.0 | 0.0 |
| FeO | 21.0 | 1.16 | 30.4 | 21.0 | 0.9 | 0.45 |
| MnO | 0.11 | 0.02 | 5.98 | 0.11 | 0.0 | 1.03 |
| MgO | 7.9 | 0.52 | 2.12 | 7.9 | 0.48 | 0.0 |
| CaO | 0.0 | 0.01 | 1.55 | 0.0 | 0.0 | 53.6 |
| $Na_2O$ | 0.17 | 0.58 | 0.0 | 0.17 | 1.18 | 0.0 |
| $K_2O$ | 8.84 | 10.4 | 0.0 | 8.84 | 9.16 | 0.0 |
| $P_2O_5$ | 0.0 | 0.0 | 0.0 | 0.0 | 0.0 | 41.7 |

* End-members of quartz, anorthite, albite, potassium feldspar, and sillimanite were assumed as phases, except for calculation of petrogenetic grid where $Or_{90}Ab_{10}$ was assumed for potassium feldspar.
† Compositions used in calculation of petrogenetic grid.
‡ Compositions used in calculation of mineral modes.

[1]For a copy of Tables 1 and 2, document item AM-99-021, contact the Business Office of the Mineralogical Society of America (see inside front cover of recent issue) for price information. Deposit items may also be available on the American Mineralogist web site (http://www.minsocam.org or current web address).

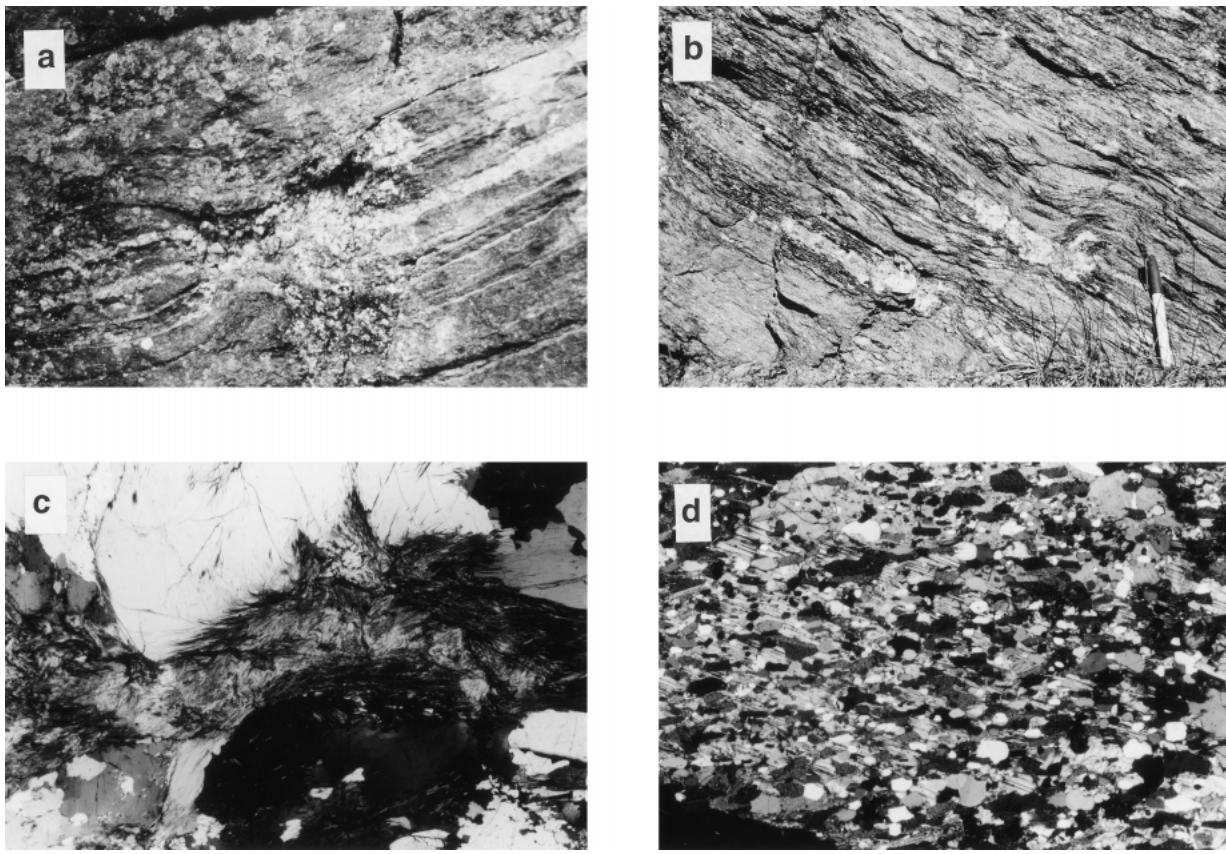


**FIGURE 2.** (**a**) Granitic leucosome segregation concentrated within a boudin neck; Horizontal dimension ~30 cm. (**b**) Additional granitic leucosome segregations. Darkest areas near and to upper left of leucosomes are biotite plus sillimanite selvages. Thin leucosomes below pen are dominated by quartz and sillimanite as in **c**. (**d**) Poikiloblastic perthite enclosing biotite and quartz. Note the alignment of biotite. Horizontal dimensions of (**a**) and (**b**) are approximately 30 cm and 65 cm, respectively, and of both (**c**) and (**d**) 7 mm.

ably by a fluid, or diffused away down chemical potential gradients within the fluid. The poikiloblastic potassium feldspar in the mesosomes is attributed to addition of the alkalis into the surrounding rock, indicating that some of the refractory mesosomes were modified during crystallization of the leucosomes (Fig. 4).

## Conditions of migmatization

The pressure and temperature conditions of migmatization were estimated from mineral compositions and assemblages. One migmatite sample, 124-1 has a pseudo-invariant assemblage in the KFMASH system, although muscovite in it is retrograde. It is the only sample in the migmatites that was found to contain garnet. Mineral compositions in sample 124-1 (Table 3) were used to calculate melt-absent reactions relevant to the migmatites using the computer program THERMOCALC with application of the Holland and Powell (1998) thermodynamic data base (Fig. 5). Mineral compositions in other migmatite samples are similar. The invariant point lies at approximately 4.5 kbar and 700 °C, placing conditions of migmatization well above the wet granite solidus. Therefore, the muscovite breakdown reaction

$$ms + q \rightarrow kfs + sil + H_2O \quad (2)$$

must have led to melting in the presence of plagioclase. Indeed, when the muscovite dehydration-melting reaction

$$ms + q + pl \rightarrow melt + sil \pm kfs \quad (3)$$

determined experimentally by Patiño-Douce and Harris (1998) on schists having compositions similar to those in the Black Hills, is extrapolated to pressures applicable to the Black Hills migmatites, it passes near the invariant point. Because under melt-present conditions the invariant point must lie on reaction 3, the calculated melt-absent reactions give reasonable estimates of pressure and temperature conditions of migmatization. The general lack of garnet in the migmatites may be related to decompression associated with emplacement of the HPG through the essentially isobaric reaction

$$grt + ms \rightarrow bt + 2\ sil + q. \quad (4)$$

In unmigmatized schists, garnet may have been stabilized by higher Mn concentrations (Table 1). The reactions indicate that partial melting in the migmatite zone occurred at *P-T* conditions bounded by the muscovite dehydration-melting reac-

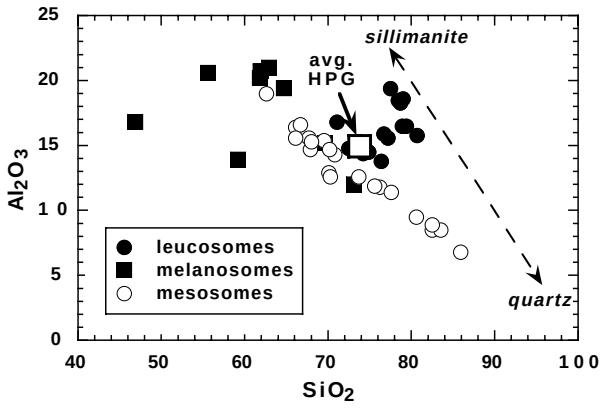


**FIGURE 3.** Covariation of $Al_2O_3$ and $SiO_2$ in Black Hills migmatites. Mesosome compositions are dominantly controlled by mixtures of quartz with micas and melanosome compositions by mixtures of biotite and sillimanite with some quartz. Removal of alkalis (mass loss) from granitic leucosomes moves composition toward quartz + sillimanite mixing line. Average composition of the Harney Peak Granite (Nabelek et al. 1992a) is shown for reference.

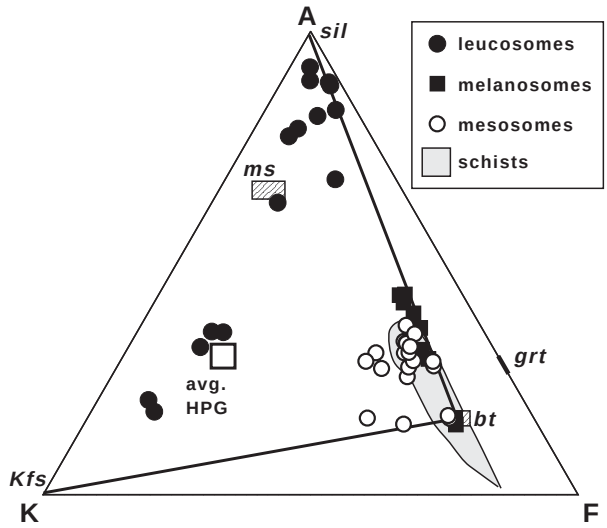


**FIGURE 4.** AKF diagram showing compositions of Black Hills migmatites. Compositions of relevant migmatite minerals (Table 3) and average Harney Peak Granite (Nabelek et al. 1992a) are shown for reference. Note that position of melanosomes relative to mesosomes requires formation of granite leucosomes. Formation of sillimanite-dominated leucosomes without previous loss of potassium cannot explain relative positions of melanosomes and mesosomes. Also note some mesosomes are anomalously enriched in K.

tion, reaction 4, and a melt-present reaction analogous to the following one:

$$sil + bt + 2q \rightarrow grt + kfs + H_2O. \quad (5)$$

During cooling, however, crystallization of leucosomes likely proceeded toward the wet granite solidus. The estimated pressure and temperature conditions for migmatization are consistent with thermobarometry on rocks below the second sillimanite isograd (Helms and Labotka 1991; Friberg et al. 1996).

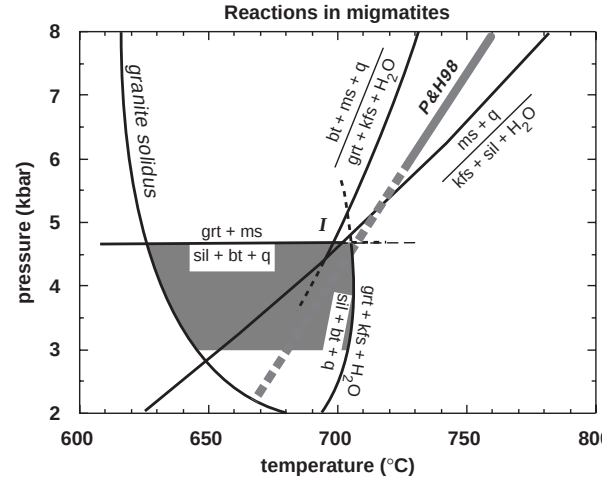


**FIGURE 5.** Petrogenetic grid relevant to Black Hills migmatites. Melt-absent reactions were calculated using mineral compositions in sample 124-1 (Table 3). Experimentally determined dehydration-melting solidus of a schist, similar in composition to Black Hills schists, by Patiño-Douce and Harris (1998) is also shown. The reaction is ms + pl + q → melt + sil + bt + kfs. The dashed part of the reaction is extrapolated. The patterned field indicates bounding pressure and temperature conditions in the migmatites, from melting at the muscovite breakdown reaction to cooling toward the wet granite solidus. Mineral abbreviations are: bt = biotite, grt = garnet, kfs = potassium feldspar, ms = muscovite, pl = plagioclase, q = quartz, sil = sillimanite.

## Trace-element systematics

The distribution of each examined trace element in the migmatites is considered in terms of the major oxide with which it is highly correlated in the schists (Appendix Table 2). Co, Zn, and Cr correlate well with MgO; Rb and Ba correlate well with $K_2O$; and Sr correlates well with $Na_2O$ (Figs. 6–8). In schists just below the second sillimanite isograd, MgO indicates the proportion of biotite, $K_2O$ the proportion of muscovite plus biotite, and $Na_2O$ the proportion of feldspar. In contrast, Cs correlates poorly with all major oxides in the schists (Appendix Table 2; Fig. 7). Nevertheless, Cs probably resides primarily in micas as there are no other minerals with sites large enough to accommodate it.

In the different migmatite parts, correlations are good, except for few samples. However, the slopes of the correlations are variable because the trace elements reside in different minerals. For example, the concentration of Ba in most leucosomes is related to amount of feldspar, whereas in the melanosomes it is related to the amount of biotite. In contrast to the migmatites and schists, in the HPG the correlations are poor (Figs. 7 and 8). This suggests trace element concentrations in the HPG were controlled by residue-melt equilibrium during partial melting coupled with fractional crystallization instead of mineral proportions (see below).

REE patterns of the leucosomes are flat at low chondrite-normalized concentrations (Fig. 9) except for one sample, 118-1-L, which has high REE (~100× chondrite) and an unusually high modal proportion of apatite (9.1%). Some patterns have large positive Eu anomalies. The leucosome REE

patterns are similar to patterns of the high-$\delta^{18}O$ granites, except that the granites never have positive Eu anomalies (Nabelek and Glascock 1995). The melanosomes, overall, have the highest REE concentrations because the bulk of monazite remained in residual biotite; melanosome and their REE patterns have large negative Eu anomalies. The mesosomes have intermediate REE patterns that are similar to those of the schists (Nabelek and Glascock 1995).

In the schists and melanosomes, Eu correlates fairly well with both $TiO_2$ and $Al_2O_3$ (Appendix Table 2). This is an indirect correlation because much of the Eu, especially $Eu^{3+}$, is in monazite inclusions in biotite. In contrast, in leucosomes most of the $Eu^{2+}$ is probably in feldspars. Therefore, the distribution of Eu is plotted against $Na_2O + K_2O$ (Fig. 10). The ratio of $Eu^{2+}/Eu^{3+}$ in the migmatites is probably high because of reducing conditions that are suggested by the presence of graphite. Note that most samples show a correlation between the magnitude of the positive Eu anomaly with the amount of feldspar, but the two most feldspar-rich samples have almost no anomaly (Fig. 10c).

## CHEMICAL RELATIONSHIP OF MIGMATITES TO LOWER GRADE ROCKS

For the purposes of modeling trace-element behavior in the migmatites, it is better to use average trace-element concentrations of the schists than of the mesosomes because some of the latter were compositionally modified as evidenced by poikiloblastic potassium feldspar. Therefore, it must be established that protoliths of the migmatites were chemically equivalent to the schists. Because of the original sedimentary nature of the rocks, the equivalence was tested by principal component analysis of major elements in the schists and mesosomes. The same four principal components describe most of the variance in both groups of rocks. The first prominent component corresponds to anticorrelation of $SiO_2$ (quartz) with oxides that make up micas, the second component to CaO and $Na_2O$ (plagioclase), the third component to MnO (mostly garnet), and the fourth component to $P_2O_5$ (phosphates). The four components describe 53.5, 17.5, 11.8, and 10.2% of the variance, respectively, in the schists and 60.5, 21.2, 10.1, and 5.8% in the mesosomes. The loadings of all oxides in the principal components are similar in both groups of rocks, except for MnO, which probably resides mostly in biotite instead of garnet above the second sillimanite isograd (Fig. 11). The similarity of loadings strongly suggests that, although the chemical variation is large in both the migmatites and schists, the average compositions of their protoliths were similar. Indeed, similar ranges of trace element concentrations in the mesosomes and schists (Figs. 6–8, 10) indicate that this was the case. Therefore, it is reasonable to use compositions of the schists as proxies for migmatite protoliths.

## EVALUATION OF RESIDUE-MELT EQUILIBRIUM

To demonstrate that trace-element distributions among the Black Hills melanosomes and leucosomes are not consistent with residue-melt equilibrium, it is useful to evaluate the distributions using mineral-melt distribution coefficients. Concentration of a trace element in a partial melt, $C_l$, is given by the equilibrium mass-balance relationship between residue and melt, $C_l = C_o/[D(1–F) + F]$ (Hanson 1978), where $C_o$ is concentration of the trace element in the parent rock, $F$ is fraction of melting, and $D = \Sigma Y_j K_j$, where $Y_j$ is proportion of mineral $j$ in the residue and $K_j$ is the distribution coefficient of the trace

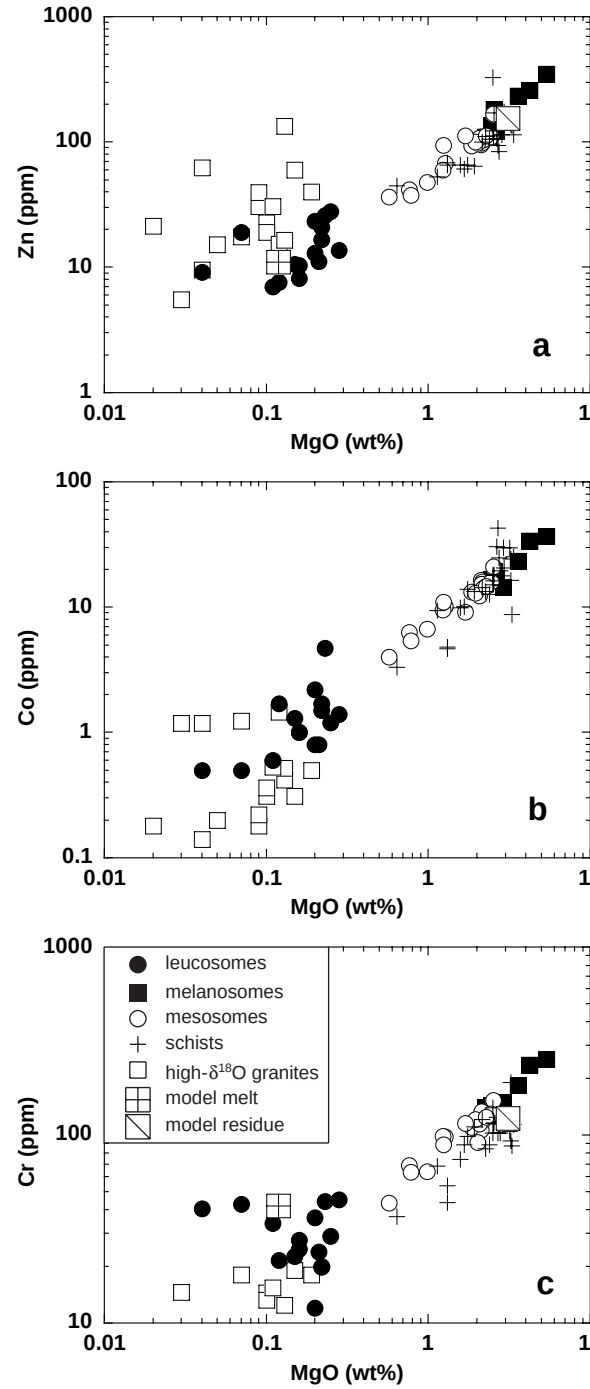


**FIGURE 6.** Covariations of period-four transition metal trace elements with MgO. Note the logarithmic scales. Model Zn (**a**) and Cr (**c**) concentrations in a model partial melt and residue are also shown. Lack of distribution coefficient data for Co (**b**) prevents calculation of model compositions.

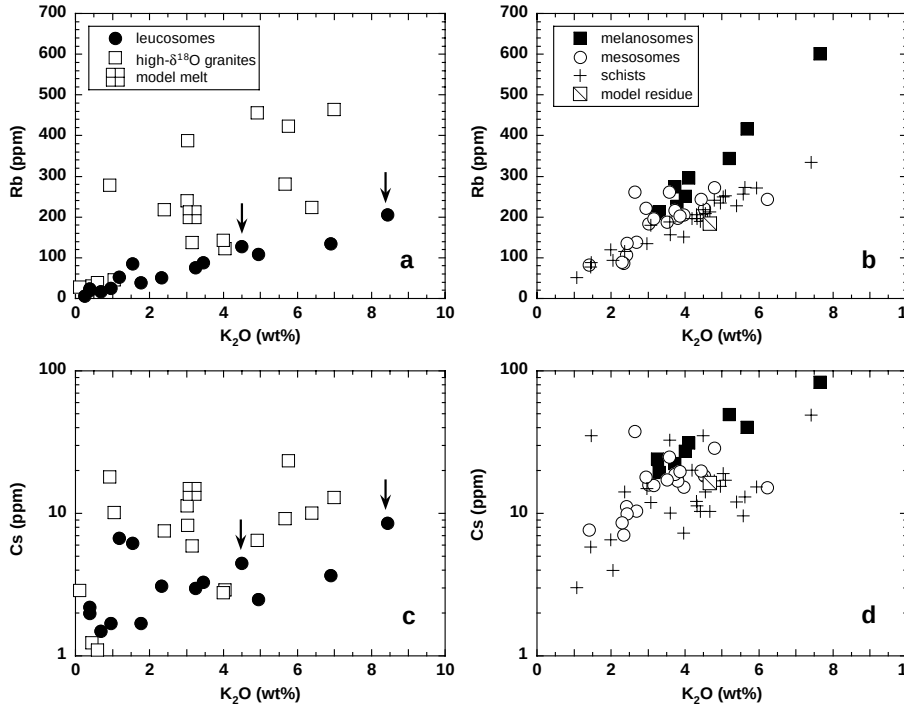


**FIGURE 7.** Covariations of Rb (**a**, **b**) and Cs (**b**, **c**) with $K_2O$ in migmatites and, for comparison, the Harney Peak Granite, model partial melt, and model residue. Concentrations of Rb and Cs are lower in leucosomes relative to the high-$\delta^{18}O$ granites and the model melt. There are good correlations of the trace elements with $K_2O$ in leucosomes. Arrows identify two samples, 115-1-L and 129-2-L, that fall off correlations in Figures 8 and 10.

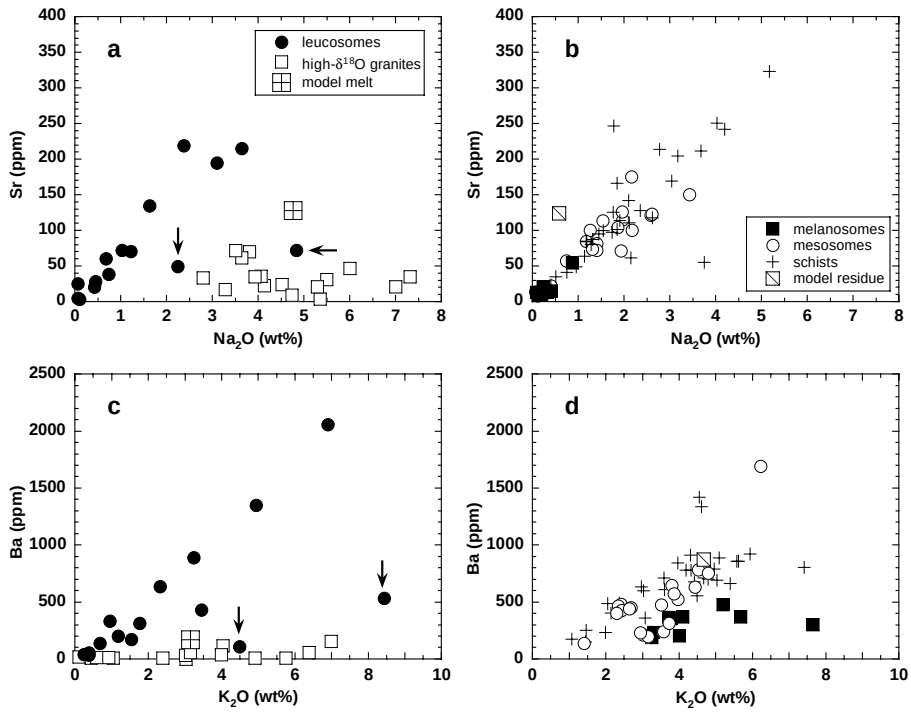


**FIGURE 8.** Covariations of Sr (**a**, **b**) and Ba (**b**, **c**) with $K_2O$ and $Na_2O$ in migmatites and, for comparison, the Harney Peak Granite, model partial melt, and model residue. Concentrations of Sr and Ba are higher in leucosomes relative to the high-$\delta^{18}O$ granites and the model melt. There are good correlations of the trace elements with the major oxides in leucosomes except for two samples, 115-1-L and 129-2-L (identified by arrows), that fall off the correlations.

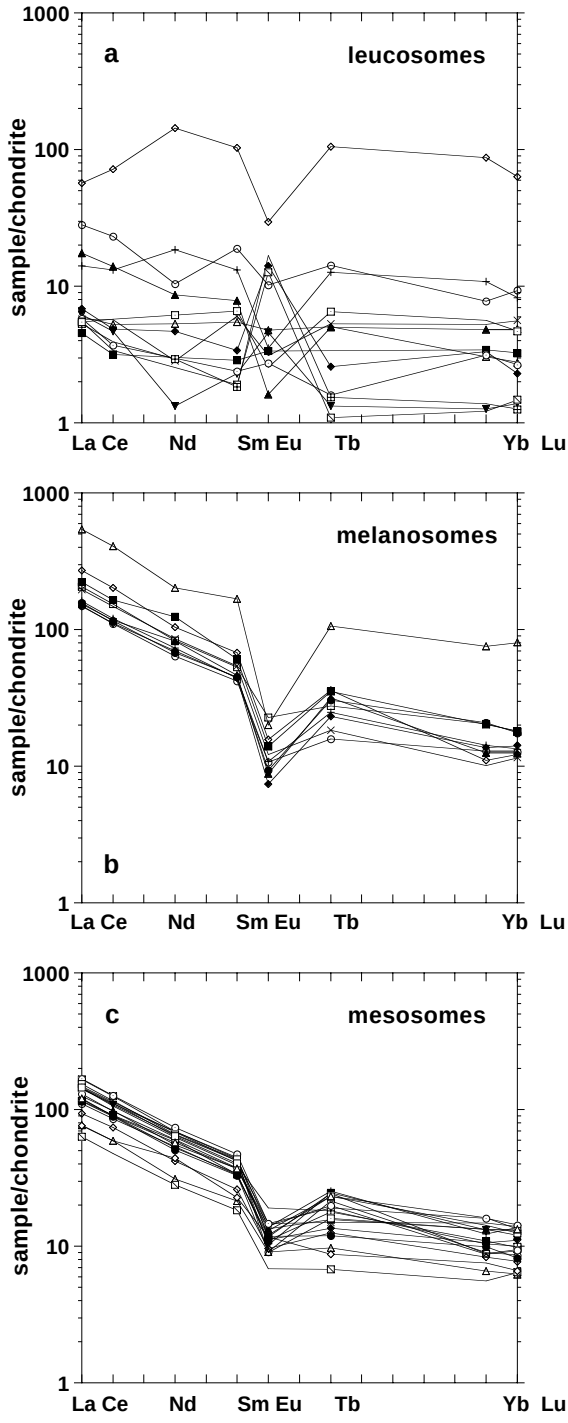


**FIGURE 9.** Chondrite-normalized rare earth element patterns in Black Hills migmatites. (**a**) Patterns of leucosomes are flat and low, except for one sample with 9.1% apatite. Most, but not all leucosomes that contain feldspar have positive Eu anomalies (Fig. 10). Apparent negative Nd anomalies are likely due to fractionation by the accessory minerals in melanosomes. (**b**) REE concentrations in melanosomes are the highest in the migmatites. (**c**) REE patterns of mesosomes are typical for pelitic rocks. Values for chondites were taken from Haskin et al. 1966).

element between mineral $j$ and melt (Table 4). Here, the values of $Y_j$ correspond to average mineral proportions in the melanosomes (43% biotite, 2% plagioclase, 4% orthoclase, 12% sillimanite, and 39% quartz) and the values of $C_o$ are average element concentrations in the schists. $F$ is assumed to be 0.25 based on the average potential fertility of the schists assuming only muscovite dehydration-melting reaction (Nabelek and Bartlett 1998). The equilibrium concentration of the trace element in the model residue, $C_s$, is given by $C_l \cdot D$. For elements compatible with respect to residue, results are relatively insensitive to a reasonable range in $F$ values.

The calculated concentrations of Cr, Co, and Zn in the model melt and residue match well those in the leucosomes and melanosomes (Fig. 6). Indeed, the good match could be interpreted to indicate that the melanosome and leucosome compositions are the result of residue-melt equilibrium, where the large differences in the relative concentrations are due to the large values of $K_{bt}$ for the transition metals (Table 4). On the other hand, there are no minerals in the leucosomes that can take up large amounts of transition metals, although sillimanite can potentially contain appreciable concentrations of Cr. The transition metals occur mostly in biotite, which is concentrated in the melanosomes. Because the transition metals also reside within biotite in rocks that have not undergone melting, the distribution of the transition metals among the melanosomes and leucosomes can also be interpreted as simply reflecting the proportion of biotite.

In contrast to the transition metals, concentrations of Rb, Cs, Ba, Sr, and Eu in the leucosomes are quite different from those in the model melt and the HPG. Except for two samples, 115-1-L and 129-2-L, which fall off correlation trends for the divalent cations (Figs. 8 and 10), the concentrations of Rb and Cs are substantially lower and those of Sr, Ba, and Eu are higher in the leucosomes than in the granite or the model melt for a given $K_2O$ or $Na_2O$ concentration. Similarly, the model residue compositions do not match compositions of the melanosomes. The Rb and Cs concentrations in the model residue are significantly lower and those of Sr and Ba are higher than in the melanosomes. These discrepancies indicate that residue-melt equilibrium was not preserved in the migmatites.

Another indication that residue-melt equilibrium was not preserved in the migmatites is in the contrasting behavior of the trace elements in the migmatites and the HPG. As shown in Figures 6–8 and 10, concentrations of the examined trace elements in the HPG do not correlate with the proportion of any mineral. The lack of correlation is consistent with partial melting of heterogeneous source rocks with variable residue mineralogy leading to small batches of melt (Nabelek and Bartlett 1998). If the composition of the leucosomes was controlled by residue-melt equilibrium, then their trace element concentrations should show similar lack of correlations with major element oxides as the HPG. Instead, the good correlations indicate a mineralogical control on the trace element distributions.

## FRACTIONAL CRYSTALLIZATION

Several investigators ascribed leucosomes with high concentrations of Sr, Ba, and REE patterns with positive Eu anomalies (as observed in some Black Hills leucosomes) to

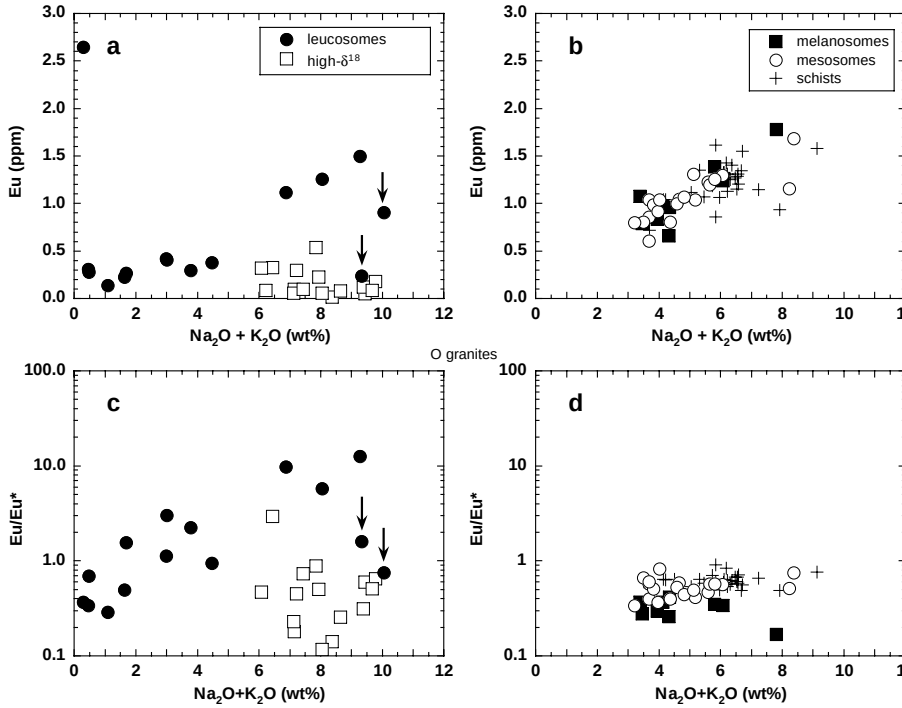


**FIGURE 10.** Covariations of Eu (**a**) and Eu/Eu* (**b**) with $K_2O + Na_2O$ in migmatites and, for comparison, the Harney Peak Granite (Nabelek and Glascock 1995). Eu/Eu* shows the extent of Eu anomaly in a REE pattern, where Eu* is extrapolated chondrite-normalized Eu concentration between Sm and Tb. Samples 115-1-L and 129-2-L, which lie off the correlations, are identified by arrows.

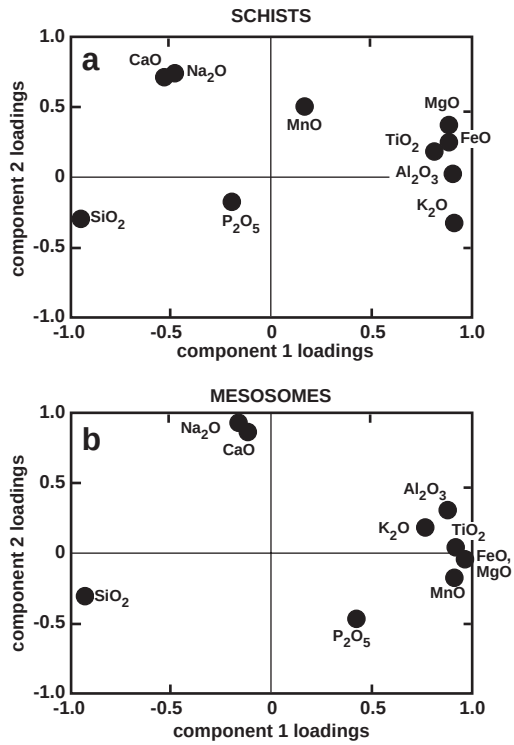


**FIGURE 11.** Loadings of oxides for first two principal components in schists (**a**) and mesosomes (**b**) based on statistical principal component analysis. Note similarity of loadings distributions in both groups of rocks.

**TABLE 4.** Trace-element distribution coefficients used in calculations

| | Rb | Cs | Sr | Ba | Cr | Zn | Eu |
|---|---|---|---|---|---|---|---|
| | | | | **mineral/melt*** | | | |
| potassium feldspar | 0.7† | 0.1 | 13† | 18† | 0.0 | 0.08 | |
| plagioclase | 0.1 | 0.1 | 13† | 1.5† | 0.0 | 2.8 | |
| biotite | 2.0‡ | 2.7 | 0.4 | 10‡ | 6.8 | 32 | |
| | | | | **mineral/potassium feldspar§** | | | |
| plagioclase | 0.02 | 0.1 | 1.6 | 0.05 | | | 1.3 |
| biotite | 2.5 | 6.4 | 0.01 | 0.16 | | | 0.02 |
| apatite | 0 | 0 | 0 | 0 | | | 10.3 |

* Mineral/melt $K_d$ values are averages from Mahood and Hildreth (1983) and Nash and Crecraft (1985), except for:
† Icenhower and London (1996);
‡ Icenhower and London (1995);
§ From data of Bea et al. (1994).

open-system fractional crystallization of feldspar from partial melts (e.g., Cuney and Barbey 1982; Sawyer 1987). Although it is very likely that the Black Hills leucosomes were modified by fractional crystallization, as evidenced for example by movement of melt to boudin necks, the following strongly indicate that the trace-element distributions in the migmatites are not simply the product of fractional crystallization of the leucosomes:

(1) Fractional crystallization of feldspar should lead to residual melts with significant negative Eu anomalies. The most likely candidates for extracted residual melts are leucosomes in boudin necks, but these typically have some of the largest positive Eu anomalies.

(2) If residue-melt equilibrium conditions are preserved during cooling of migmatites, then fractional crystallization of

leucosomes should have no effect on the composition of melanosomes. However, the calculated Rb, Cs, Sr, and Ba concentrations in the model residue do not match those in melanosomes, even though the melanosome mineralogy was used in determining mineral-melt distribution coefficients. As will be demonstrated below, the melanosomes did not remain chemically isolated from processes in the crystallizing leucosomes.

## EVALUATION OF SOLID-STATE EQUILIBRIUM

There are two ways by which mineral-mineral equilibrium could have been established between leucosomes and melanosomes. In the first way, equilibrium was established by diffusion during protracted cooling of a migmatite terrane only after partial melts crystallized without chemical interaction with melanosomes. This is essentially the model that was proposed by Fourcade et al. (1992) for equilibration in the St. Malo migmatites. In the second, the preferred way, mineral-mineral equilibrium was established during crystallization of leucosomes.

### Post-crystallization equilibration

For the achievement of trace-element equilibrium between minerals through volume diffusion, the minerals must be for sufficient time above the blocking temperatures for diffusion. To estimate the period of time the Black Hills migmatites were above the blocking temperatures of the considered elements, a temperature-time path was calculated for rocks above the second-sillimanite isograd at a distance of 500 m from contact with HPG (Fig. 12a). The values of input parameters are also shown in Figure 12a. It was assumed that the schists were at 500 °C at the time of HPG emplacement, which is the maximum temperature estimated by Holm et al. (1997) from $^{40}Ar/^{39}Ar$ data. Selecting a lower temperature would lead to faster cooling and therefore a smaller diffusion distance. The temperature of intrusion was assumed to be 850 °C, consistent with temperatures of dehydration-melting reactions at high pressures and the liquidus of the HPG (Nabelek and Ternes 1997). The calculated path shows that the rocks would have been above 600 °C for ~4 Ma, followed by cooling to 570 °C at an average rate of ~6.7 °C and then at a rate of 4.5 °C. These results can be used to estimate the extent of equilibration of trace elements among minerals in the migmatites.

The diffusion of Sr into orthoclase is used here as an example. There are two sets of experimental results for diffusion of Sr in orthoclase. The results of Giletti (1991; $D_o = 5.97 \times 10^{-7}$ m$^2$/s, $E_a = 167.360$ kJ/mol) are for self-diffusion, which involves the exchange of Sr from an external source for Sr already in the crystal structure. The results of Cherniak and Watson (1992; $D_o = 2.5 \times 10^{-6}$ m$^2$/s, $E_a = 284.083$ kJ/mol) are for chemical diffusion, which involves the net addition of Sr into the crystal structure. Chemical diffusion is rate-limited by the movement of network-forming Al and Si to preserve charge balance and is therefore much slower than self-diffusion. Equilibration of feldspars in migmatites that is modeled here would more likely have involved chemical diffusion, as there would have been net addition of Sr into the feldspars that initially crystallized from a low-Sr melt indicated by composition of the HPG and the model partial melt (Fig. 8). On the other hand, the experiments of Giletti (1991) were done under hydrothermal conditions, analogous to likely subsolidus conditions in the migmatites.

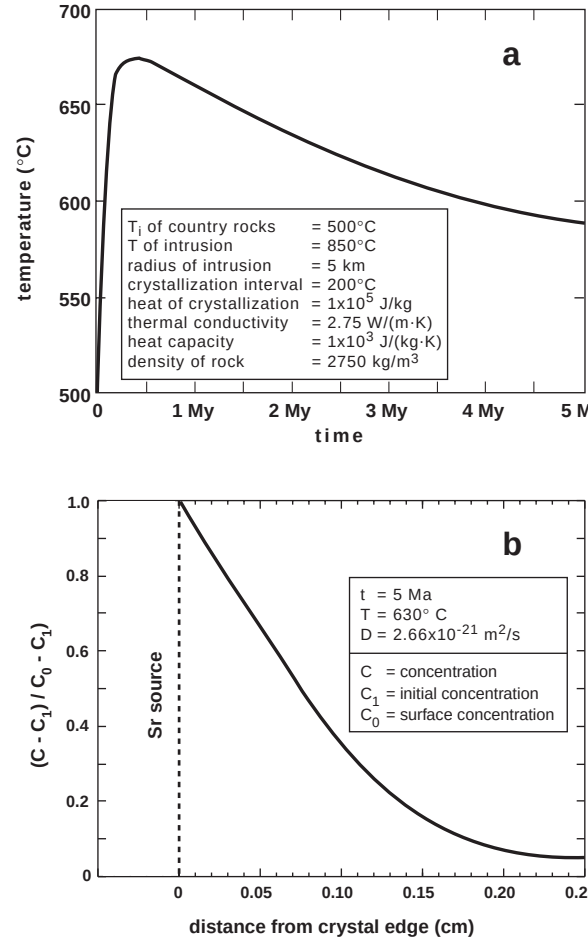


**FIGURE 12.** (**a**) Theoretical temperature-time path for country rocks 500 m from Harney Peak Granite contact following granite intrusion. (**b**) Theoretical Sr concentration profile in potassium feldspar that would result from Sr equilibration among migmatite minerals while rocks were above the blocking temperature for diffusion.

For a grain 0.25 cm in diameter and cooling rate of 6.7 °C/Ma, application of the equation of Dodson (1973) yields blocking temperature of 726 °C using values of diffusion parameters of Cherniak and Watson (1992) and 586 °C using the values of Giletti (1991). The former result implies that Sr concentrations acquired by orthoclase during its crystallization from melt should be preserved through cooling of migmatites, whereas the latter result implies that diffusion of Sr into the orthoclase structure during subsolidus cooling could occur. For the latter result, the extent of plausible Sr diffusion into orthoclase was calculated assuming tracer diffusion into a sphere (Crank 1975, p. 91). The calculated profile for 630 °C and 5 Ma, the approximate average temperature and time that the Black Hills migmatites spent above the 586 °C blocking temperature (Fig. 12a), shows that Sr in orthoclase should be strongly zoned (Fig. 12b). Similar profiles

are obtained for Sr diffusion in albite and Ba diffusion in orthoclase. They suggest that equilibration of the Black Hills leucosomes with melanosomes during subsolidus cooling alone at best would have led to poor correlations of Sr and Ba with $Na_2O$ and $K_2O$, respectively. It is concluded, therefore, that equilibration during subsolidus cooling was not the principal cause of the very good correlations and the enhanced Sr, Ba, and Eu concentrations in the leucosomes above those in the HPG and model melt (Figs. 8 and 10).

**Syn-crystallization equilibration**

Solid-state equilibrium in migmatites also can be established during crystallization of leucosomes if they maintain equilibrium with surrounding melanosomes. As discussed above, partial melting by reaction 3 occurs above the temperature of the water-saturated granite solidus at 3.5 kbar. Therefore, crystallization of the partial melts will proceed to lower temperatures than the solidus of a metapelite. The crystallization will lead to potassium feldspar instead of muscovite as the major K-bearing phase in leucosomes. The resulting assemblage in a melanosome-leucosome pair will be the same as would result from prograde reaction 2. With the exception of few samples with retrograde muscovite, this is the case in the Black Hills migmatites. Thus, for the purposes of modeling the Black Hills migmatites, it can be assumed that their mineralogy is the product of reaction 2. Plagioclase and biotite can be considered to have been passive participants during migmatite formation, the former being distributed among corresponding leucosomes and melanosomes and the latter becoming concentrated in the melanosomes.

A reaction-progress approach that was developed originally by Chamberlain et al. (1990) for oxygen isotope fractionation during net-transfer reactions is modified here for trace elements to determine if the distribution of Rb, Cs, Sr, Ba, and Eu in the migmatites represents mineral-mineral equilibrium. The method combines mineral reaction-progress with trace-element mass-balance constrained by mineral/mineral distribution coefficients. The proportion of a mineral $i$ during a net-transfer reaction is given by

$$X_i = \frac{\nu_i a_i \zeta + a_i n_i}{a_i n_i + \sum_j a_j n_j} \qquad (6)$$

where $\nu$ is the stoichiometric coefficient of $i$ in the reaction, $a$ is molecular weight of a mineral, $n$ is number of moles of the mineral before the reaction, $\zeta$ is the reaction progress variable, here assumed to be equal to 1 (i.e., reaction 1 went to completion), and $j$ refers to all minerals other than $i$. The concentration of a trace element in the mineral $i$, assumed to be potassium feldspar in the calculations, is given by:

$$C_i = \frac{C_o}{1 - \sum_j X_j + \sum_j D_j X_j} \qquad (7)$$

where $D_j$ is the distribution coefficient between a mineral $j$ and the mineral $i$. The concentration in another mineral is given by $C_j = C_i \cdot D_j$. Mineral/Kfp distribution coefficients (Table 4) were extracted from the data of Bea et al. (1994) assuming $D_j = C_j/C_{lc} \cdot C_{lc}/C_{kfs}$, where $C_{lc}$ is concentration in leucosome. The number of moles of each mineral before reaction was calculated from the average mode of the schists (35% quartz, 14% muscovite, 20% plagioclase, 29% biotite, and 0.25% apatite). The reaction coefficients were those of reaction 2 with coefficients for minerals not partaking in the reaction, biotite and plagioclase, set to zero. The initial values of the $C_o$ terms were set equal to the average trace element concentrations of schists from the Black Hills: (i.e., Rb = 190 ppm, Cs = 15.8 ppm, Sr = 126 ppm, Ba = 699 ppm, and Eu = 1.22 ppm). The logic behind using the average mode and trace element concentrations of the schists is based on the strong correlations of the considered elements with $K_2O$ or $Na_2O$. Therefore, for example, a rock that initially had more muscovite than the average schist also had proportionately more Ba than the average schist. Following reaction at the second sillimanite isograd, the initially higher amount of muscovite must have translated into an equivalent amount of potassium feldspar. These assumptions are not entirely appropriate for Eu, because a portion of it resides in monazite, which was unreactive during partial melting (Nabelek and Glascock 1995). The assumptions may hold, however, for $Eu^{2+}$.

The model was tested (see Fig. 13) by comparing the observed trace element concentrations with model concentrations of Rb, Cs, Ba, Sr, and Eu in the bulk leucosomes and melanosomes, calculated from the values of $C_i$ and modal mineral proportions (Appendix Table 1). With the exception of samples 115-1-L and 129-2-L, the correspondence is good to excellent for the five elements tested. There is very little difference between model and observed concentrations of Sr and Ba. Although the correspondence trends for Rb are very linear, the model concentrations somewhat underestimate the observed concentrations of both leucosomes and melanosomes. This may be because the assumed $C_o$(Rb) was too low. Assumption of 220 ppm for $C_o$(Rb) would have yielded an excellent correspondence. The model Eu concentrations of leucosomes are higher and of the melanosomes lower than the observed concentrations, although the leucosome trend is fairly linear. The discrepancy is attributed to a significant proportion of Eu being in monazite, which was not accounted for in the calculation, within the melanosomes. The use of average schist modes and the implicit assumption of closed-system behavior also may have contributed to some discrepancies for all the examined elements. However, the reaction-progress method minimizes discrepancies due to open-system behavior, such as fractional crystallization of leucosomes, because only mineral modes of the migmatites, not their compositions, are used in calculating the model concentrations.

The overall correspondence between model and observed concentrations of the five trace elements in the leucosomes and melanosomes implies that equilibrium was maintained between crystallizing partial melts and melanosomes. Equilibration was likely enhanced by the presence of fluids, either melt or vapor phase that was exsolving from the crystallizing melts. Evident coarsening of melanosome biotite indicates such equilibration. Only samples 115-1-L and 129-2-L fall significantly off the correlations for most of the five modeled elements. Their observed trace element compositions correspond more to compositions of the model melt and the HPG (Figs. 8 and 10). These leucosomes

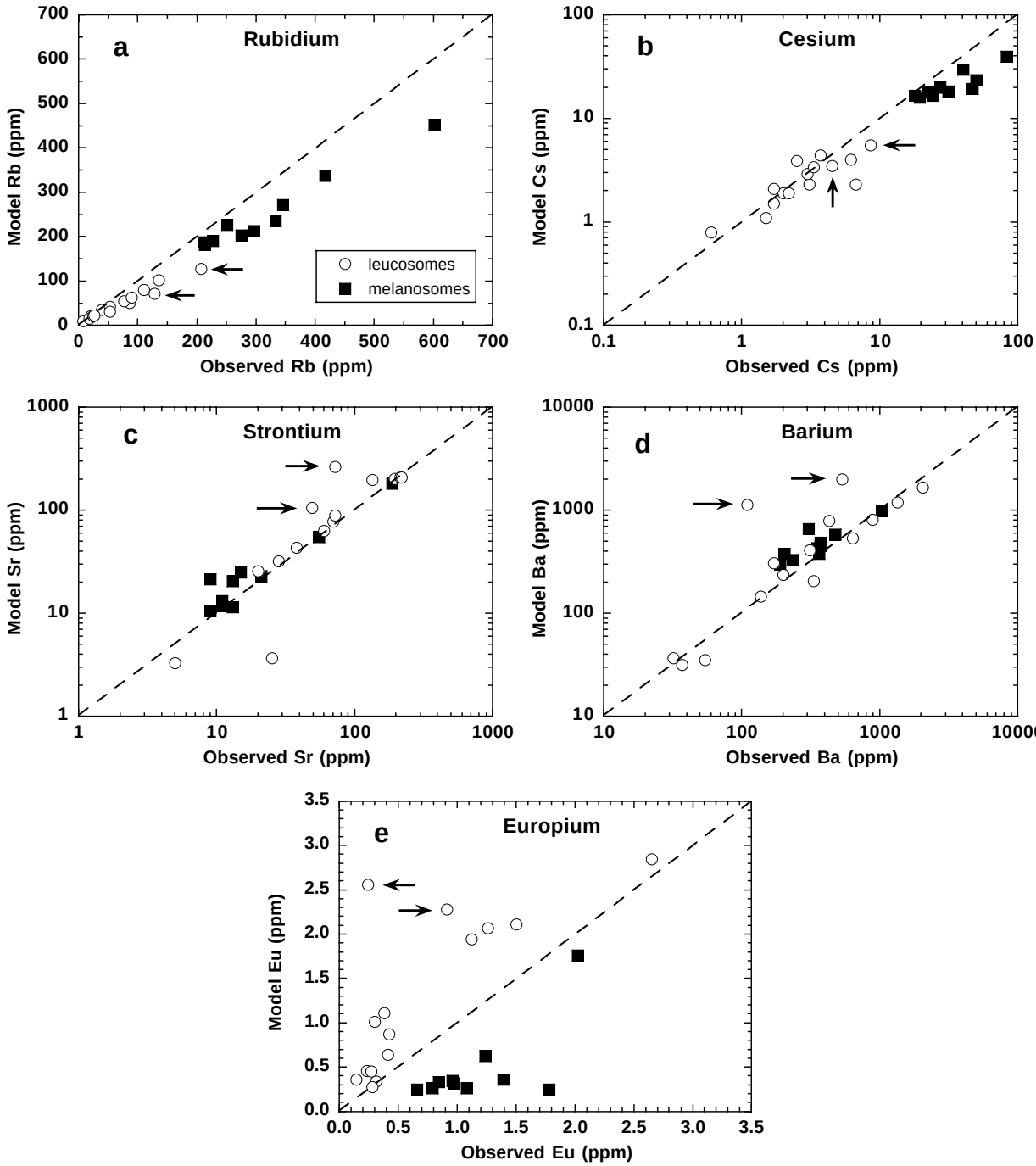


**FIGURE 13.** Model concentrations of Rb (**a**), Cs (**b**), Sr (**c**), Ba (**d**), and Eu (**e**) in leucosomes and melanosomes, calculated assuming solid state equilibrium, are compared to observed concentrations. There is good correspondence between model and observed concentrations of the alkali and alkali earth elements for most samples. Samples 115-1-L and 129-2-L that plot near compositions of the HPG in Figures 8 and 10 are identified by arrows. Compositions of these two samples suggests that they are either partial melts that did not achieve solid state equilibrium during crystallization or are intruded granites. Model Eu concentrations for leucosomes are consistently higher than observed concentrations and the converse is true for melanosomes. This is because monazite and other REE rich accessory minerals that are concentrated in melanosomes were not accounted for in the model.

could not have equilibrated with melanosomes. However, it is more likely that they are intruded HPG melts because they do not have obvious melanosome selvages, even though they are concordant to foliation. Thus, the reaction-progress method provides a means for determining if intruded or locally generated melts equilibrated with the surrounding rock during crystallization.

## Concluding Remarks

Results of this study indicate that the distributions of Rb, Cs, Ba, Sr, $Eu^{2+}$, and period-four transition metals between melanosomes and leucosomes in migmatites can approach solid-state equilibrium. The equilibrium is more likely achieved during crystallization of partial melts leading to leucosomes than by subsolidus eradication of residue-melt equilibrium that is established during partial melting (cf. Fourcade et al. 1992). If solid-state equilibrium is common in migmatites, as suggested for example by the occurrences of positive Eu anomalies in REE patterns of leucosomes in many terranes (Sawyer 1987; Johannes et al. 1995; Watt and Harley 1993; Watt et al. 1996; Carrington and Watt 1995), then inferences from trace element distributions in migmatites about melt-forming processes in the crust, such as identification of melt-forming reactions or kinetics or melting and melt extraction, may be difficult. In addition, the behavior of trace elements hosted dominantly by major rock-forming minerals may be quite different from those hosted mainly by accessory minerals such as monazite. Whereas the equilibrium of the former may adjust to new conditions throughout the migmatization process, as this study suggests, the latter may not participate to an appreciable extent even during the first stage of migmatite formation, partial melting (Nabelek and Glascock 1996; Bea 1996).

## Acknowledgments

Cindy Bartlett and Michael Glascock, University of Missouri, conducted INAA analyses and Rex Couture, Washington University, did the XRF analyses. Dan Kremser, Washington University, helped with electron microprobe analysis. Mona Sirbescu commented on the manuscript. The paper was significantly improved by careful and constructive comments of two anonymous reviewers. This study was supported by NSF grant EAR-9417979.

## References Cited

Bea, F. (1996) Residence of REE, Y, Th and U in granites and crustal protoliths; Implications for the chemistry of crustal melts. Journal of Petrology, 37, 521–552.

Bea, F., Pereira, M.D., and Stroh, A. (1994) Mineral/leucosome trace-element partitioning in a peraluminous migmatite (a laser ablation-ICP-MS study). Chemical Geology, 117, 291–312.

Brown, M. (1994) The generation, segregation, ascent and emplacement of granite magma: the migmatite-to-crustally-derived granite connection in thickened orogens. Earth Science Reviews, 36, 83–130.

Brown, M. and D'Lemos, R.S. (1991) The Caledonian granites of Mancellia, northeast Armorican Massif of France: relationship to the St. Malo migmatite belt, petrogenesis and tectonic setting. Precambrian Research, 51, 393–427.

Carrington, D.P. and Watt, G.R. (1995) A geochemical and experimental study of the role of K-feldspar during water-undersaturated melting of metapelites. Chemical Geology, 122, 59–76.

Chamberlain, C.P., Ferry, J.M., Rumble, D., III. (1990) The effect of net-transfer reactions on the isotopic compositions of minerals. Contributions to Mineralogy and Petrology, 105, 322–336.

Cherniak, D.J. and Watson, E.B. (1992) A study of strontium diffusion in K-feldspar, Na-K feldspar and anorthite using Rutherford backscattering spectroscopy. Earth and Planetary Science Letters, 113, 411–425.

Crank, J. (1975) The Mathematics of Diffusion (2nd edition), 414 p. Oxford Univ. Press, Oxford, U.K.

Cuney, M. and Barbey, P. (1982) Mise en evidence de phenomenes de cristallisation fractionnee dans les migmatites. Comptes-Rendus des Seances de l'Academie des Sciences, Serie 2, 295, 37–42.

Dahl, P.S. and Frei, R. (1998) Step-leach Pb-Pb dating of inclusion-bearing garnet and staurolite, with implications for Early Proterozoic tectonism in the Black Hills collisional orogen, South Dakota, United States. Geology, 26, 111–114.

Dahl, P.S., Frei, R., and Dorais, M.J. (1998) When did the Wyoming Province collide with Laurentia?: New clues from step-leach Pb-Pb dating of garnet independent of its inclusions. Geological Society of America Abstracts with Programs, 30, 109.

DeWitt, E., Redden, J.A., Buscher, D., and Burack-Wilson, A. (1989) Geologic map of the Black Hills area, South Dakota and Wyoming. U.S. Geological Survey. Map I-1910.

Dodson, M.H. (1973) Closure temperature in cooling geochronological and petrological systems. Contributions to Mineralogy and Petrology, 40, 259–274.

Fourcade, S., Martin, H., and de Brémond d'Ars, J. (1992) Chemical exchange in migmatites during cooling. Lithos, 28, 43–53.

Friberg, L.M., Dahl, P.S., and Terry, M.P. (1996) Thermometric evolution of early Proterozoic metamorphic rocks from the southern Black Hills, South Dakota. In C.J. Paterson, and J.G. Kirchner, Eds., Guidebook to the Geology of the Black Hills, South Dakota, p. 191–199. S.D. School of Mines and Technology Bulletin, Rapid City, South Dakota.

Giletti, B.J. (1991) Rb and Sr diffusion in alkali feldspars, with implications for cooling histories of rocks. Geochimica et Cosmochimica Acta, 55, 1331–1343.

Hanson, G.H. (1978) The application of trace elements to the petrogenesis of igneous rock of granitic composition. Earth and Planetary Science Letters, 38, 26–43.

Haskin, L.A., Frey, F.A., Schmitt, R.A., and Smith, R.H. (1966) Meteoritic, solar and terrestrial rare earth distributions. Physics and Chemisty of the Earth, 7, 167–321.

Helms, T.S. and Labotka, T.C. (1991) Petrogenesis of Early Proterozoic pelitic schists of the southern Black Hills, South Dakota: Constraints on regional low-pressure metamorphism. Geological Society of America Bulletin, 103, 1324–1334.

Holland, T.J.B. and Powell R. (1998) An internally-consistent thermodynamic dataset for phases of petrological interest. Journal of Metamorphic Geology, 16, 309–343.

Holm, D.K., Dahl, P.S., and Lux, D.R. (1997) $^{40}Ar/^{39}Ar$ evidence for Middle Proterozoic (1300–1500 Ma) slow cooling of the southern Black Hills, South Dakota, midcontinent, North America: Implications for Early Proterozoic P-T evolution and posttectonic magmatism. Tectonics, 16, 609–622.

Icenhower, J. and London, D. (1995) An experimental study of element partitioning among biotite, muscovite, and coexisting peraluminous silicic melt at 200 MPa ($H_2O$). American Mineralogist, 80, 1229–1251.

——(1996) Experimental partitioning of Rb, Cs, Sr, and Ba between alkali feldspar and peraluminous melt. American Mineralogist, 81, 719–734.

Johannes, W., Holtz, F., and Möller, P. (1995) REE distribution in some layered migmatites: constraints on their petrogenesis. Lithos, 35, 139–152.

Krogstad, E.J., and Walker, R.J. (1996) Evidence of heterogeneous crustal sources: the Harney Peak Granite, South Dakota, U.S.A. Transactions of the Royal Society of Edinburgh: Earth Sciences, 87, 331–337.

Krogstad, E.J., and Walker, R.J., Nabelek, P.I., and Russ-Nabelek, C. (1993) Lead isotopic evidence for mixed sources of Proterozoic granites and pegmatites, Black Hills, South Dakota, USA. Geochimica et Cosmochica Acta, 57, 4667–4685.

Mahood, G. and Hildreth, W. (1983) Large partition coefficients for elements in high-silica rhyolites. Geochimica et Cosmochimica Acta, 47, 11–30.

Nabelek, P.I. (1997) Quartz-sillimanite leucosomes in high-grade schists, Black Hills, South Dakota: A perspective on the mobility of Al in high-grade metamorphic rocks. Geology, 25, 995–998.

Nabelek, P.I. and Bartlett, C.D. (1998) Petrologic and geochemical links between the post-collisional Proterozoic Harney Peak leucogranite, South Dakota, USA, and its source rocks. Lithos, 45, 71–85.

Nabelek, P.I. and Glascock, M.D. (1995) REE-depleted leucogranites, Black Hills, South Dakota: a consequence of disequilibrium melting of monazite-bearing schists. Journal of Petrology, 36, 1055–1071.

Nabelek, P.I. and Ternes, K. (1997) Fluid inclusions in the Harney Peak Granite, Black Hills, South Dakota, USA: Implications for solubility and evolution of magmatic volatiles and crystallization of leucogranite magmas. Geochimica et Cosmochimica Acta, 61, 1447–1465.

Nabelek, P.I., Russ-Nabelek, C., and Denison, J.R. (1992a) The generation and crystallization conditions of the Proterozoic Harney Peak leucogranite, Black Hills, South Dakota, USA: Petrologic and geochemical constraints. Contributions to Mineralogy and Petrology, 110, 173–191.

Nabelek, P.I., Russ-Nabelek, C., and Haeussler, G.T. (1992b) Stable isotope evidence for the petrogenesis and fluid evolution in the Proterozoic Harney Peak leucogranite, Black Hills, South Dakota. Geochimica et Cosmochimica Acta, 56, 403–417.

Nabelek, P.I., Sirbescu, M., and Liu, M. (1999) Petrogenesis and tectonic context of the Harney Peak Granite, Black Hills, South Dakota. Rocky Mountain Geology, in press.

Nash, W.P. and Crecraft, H.R. (1985) Partition coefficients for trace elements in silicic magmas. Geochimica et Cosmochimica Acta, 49, 2309–2322.

Patiño-Douce, A.E., and Harris, N. (1998) Experimental Constraints on Himalayan Anatexis. Journal of Petrology, 39, 689–710.

Power, G.M. (1993) Geochemical differences between the Cadomian granites of Mancellia and the St. Malo migmatites, Armorican Massif, France. Journal of the Geological Society, London, 150, 465–468.

Redden, J.A., Peterman, Z.E., Zartman, R.E., and DeWitt, E. (1990) U-Th-Pb zircon and monazite ages and preliminary interpretation of the tectonic development of Precambrian rocks in the Black Hills. In J.F. Lewry and M.R. Stauffer, Eds., The Early Proterozoic Trans-Hudson Orogen, Geological Association of Canada Special Paper, 37, 229–251.

Sawyer, E.W. (1987) The role of partial melting and fractional crystallization in determining discordant migmatite leucosome compositions. Journal of Petrology, 28, 445–473.

——(1991) Disequilibrium melting and the rate of melt-residuum separation during migmatization of mafic rocks from the Grenville Front, Quebec. Journal of Petrology, 32, 701–738.

Shearer, C.K., Papike, J.J., Redden, J.A., Simon, S., Walker, R.J., and Laul, J.C. (1987) Origin of pegmatitic granite segregations, Willow Creek, Black Hills, South Dakota. Canadian Mineralogist, 25, 159–171.

Watt, G.R., Burns, I.M., and Graham, G.A. (1996) Chemical characteristics of migmatites: accessory phase distribution and chemical evidence for fast melt segregation rates. Contributions to Mineralogy and Petrology, 125, 100–111.

Watt, G.R. and Harley, S.L. (1993) Accessory phase controls on the geochemistry of crustal melts and restites produced during water-undersaturated partial melting. Contributions to Mineralogy and Petrology, 11, 550–566.

MANUSCRIPT RECEIVED JUNE 22, 1998
MANUSCRIPT ACCEPTED APRIL 30, 1999
PAPER HANDLED BY GRAY E. BEBOUT

**APPENDIX TABLE 1.** Calculated modes in leucosomes and melanosomes

| Sample | Qtz | Ab | An | Or | Bt | Sil | Ap |
|---|---|---|---|---|---|---|---|
| | | | **leucosomes** | | | | |
| 115-1 | 0.29 | 0.14 | 0.00 | 0.48 | 0.03 | 0.05 | 0.01 |
| 118-1 | 0.66 | 0.01 | 0.00 | 0.01 | 0.02 | 0.23 | 0.09 |
| 121-1 | 0.66 | 0.01 | 0.00 | 0.00 | 0.04 | 0.28 | 0.01 |
| 121-2 | 0.58 | 0.10 | 0.01 | 0.09 | 0.03 | 0.19 | 0.01 |
| 124-1 | 0.52 | 0.19 | 0.01 | 0.06 | 0.07 | 0.15 | 0.00 |
| 125-1A | 0.34 | 0.26 | 0.02 | 0.28 | 0.03 | 0.06 | 0.01 |
| 127-1 | 0.64 | 0.04 | 0.00 | 0.03 | 0.02 | 0.27 | 0.00 |
| 129-1B | 0.59 | 0.06 | 0.01 | 0.12 | 0.03 | 0.20 | 0.00 |
| 131-1B | 0.40 | 0.31 | 0.04 | 0.18 | 0.03 | 0.04 | 0.00 |
| 132-1A | 0.32 | 0.20 | 0.02 | 0.40 | 0.02 | 0.03 | 0.00 |
| 133-1A | 0.66 | 0.04 | 0.00 | 0.05 | 0.04 | 0.21 | 0.01 |
| 118-2 | 0.67 | 0.00 | 0.00 | 0.00 | 0.04 | 0.28 | 0.01 |
| 129-2 | 0.23 | 0.41 | 0.02 | 0.25 | 0.02 | 0.05 | 0.01 |
| 133-2 | 0.52 | 0.09 | 0.00 | 0.18 | 0.04 | 0.16 | 0.01 |
| 133-3 | 0.60 | 0.06 | 0.01 | 0.04 | 0.02 | 0.27 | 0.00 |
| | | | **melanosomes** | | | | |
| 115-1 | 0.38 | 0.01 | 0.00 | 0.06 | 0.36 | 0.19 | 0.00 |
| 118-1 | 0.37 | 0.00 | 0.00 | 0.03 | 0.59 | 0.02 | 0.01 |
| 121-1 | 0.57 | 0.00 | 0.00 | 0.03 | 0.31 | 0.08 | 0.00 |
| 126-5 | 0.39 | 0.03 | 0.00 | 0.04 | 0.35 | 0.20 | 0.00 |
| 127-1 | 0.18 | 0.00 | 0.00 | 0.04 | 0.79 | 0.00 | 0.00 |
| 128-1 | 0.43 | 0.01 | 0.00 | 0.06 | 0.32 | 0.18 | 0.00 |
| 129-1A | 0.26 | 0.07 | 0.01 | 0.07 | 0.46 | 0.13 | 0.00 |
| 131-1B | 0.38 | 0.02 | 0.00 | 0.03 | 0.39 | 0.17 | 0.00 |
| 132-1A | 0.52 | 0.01 | 0.00 | 0.02 | 0.33 | 0.12 | 0.00 |

**APPENDIX TABLE 2:** Correlation coefficients of oxides and trace elements in schists

| | $SiO_2$ | $TiO_2$ | $Al_2O_3$ | FeO | MnO | MgO | CaO | $Na_2O$ | $K_2O$ | $P_2O_5$ | LOI |
|---|---|---|---|---|---|---|---|---|---|---|---|
| $TiO_2$ | –0.82 | | | | | | | | | | |
| $Al_2O_3$ | –0.93 | 0.82 | | | | | | | | | |
| FeO | –0.87 | 0.63 | 0.68 | | | | | | | | |
| MnO | –0.21 | –0.03 | –0.01 | 0.46 | | | | | | | |
| MgO | –0.90 | 0.71 | 0.72 | 0.91 | 0.32 | | | | | | |
| CaO | 0.30 | –0.28 | –0.40 | –0.37 | 0.13 | –0.20 | | | | | |
| $Na_2O$ | 0.26 | –0.13 | –0.32 | –0.37 | –0.03 | –0.23 | 0.82 | | | | |
| $K_2O$ | –0.79 | 0.66 | 0.80 | 0.68 | –0.06 | 0.67 | –0.64 | –0.69 | | | |
| $P_2O_5$ | 0.16 | –0.12 | –0.09 | –0.27 | 0.05 | –0.25 | 0.14 | –0.08 | –0.06 | | |
| LOI | –0.64 | 0.52 | 0.72 | 0.48 | –0.17 | 0.47 | –0.65 | –0.61 | 0.79 | 0.02 | |
| Rb | –0.76 | 0.60 | 0.78 | 0.66 | –0.09 | 0.64 | –0.65 | –0.70 | 0.97 | –0.08 | 0.77 |
| Cs | –0.13 | –0.01 | 0.09 | 0.17 | –0.12 | 0.11 | –0.29 | –0.34 | 0.37 | –0.13 | 0.26 |
| Sr | 0.16 | –0.09 | –0.30 | –0.22 | 0.04 | –0.05 | 0.88 | 0.80 | –0.51 | –0.03 | –0.60 |
| Ba | –0.63 | 0.53 | 0.58 | 0.67 | 0.12 | 0.58 | –0.48 | –0.50 | 0.67 | –0.07 | 0.57 |
| Th | 0.12 | –0.23 | 0.01 | –0.11 | –0.16 | –0.28 | –0.33 | –0.37 | 0.18 | 0.01 | 0.12 |
| U | –0.15 | 0.29 | 0.20 | 0.10 | –0.16 | 0.10 | 0.01 | –0.09 | 0.12 | –0.16 | 0.02 |
| Sc | –0.91 | 0.88 | 0.85 | 0.77 | 0.13 | 0.85 | –0.20 | –0.13 | 0.65 | –0.23 | 0.52 |
| Co | –0.64 | 0.47 | 0.53 | 0.71 | 0.52 | 0.66 | –0.28 | –0.21 | 0.41 | –0.12 | 0.28 |
| Cr | –0.82 | 0.91 | 0.82 | 0.59 | –0.02 | 0.72 | –0.12 | 0.02 | 0.53 | –0.21 | 0.45 |
| Pb | –0.07 | –0.06 | –0.13 | 0.20 | 0.39 | 0.23 | 0.42 | 0.50 | –0.34 | –0.26 | –0.28 |
| Zn | –0.65 | 0.49 | 0.68 | 0.51 | 0.11 | 0.56 | –0.23 | –0.26 | 0.50 | –0.12 | 0.54 |
| Ni | –0.76 | 0.80 | 0.72 | 0.62 | 0.10 | 0.72 | –0.29 | –0.03 | 0.51 | –0.21 | 0.46 |
| V | –0.78 | 0.84 | 0.71 | 0.69 | 0.07 | 0.78 | –0.25 | –0.22 | 0.63 | –0.28 | 0.44 |
| Nb | –0.68 | 0.75 | 0.70 | 0.56 | –0.16 | 0.58 | –0.54 | –0.48 | 0.80 | –0.10 | 0.67 |
| Ta | –0.50 | 0.55 | 0.56 | 0.37 | –0.03 | 0.36 | –0.42 | –0.53 | 0.70 | 0.17 | 0.53 |
| Hf | 0.80 | –0.53 | –0.66 | –0.79 | –0.34 | –0.84 | 0.27 | 0.27 | –0.63 | 0.29 | –0.47 |
| Zr | 0.75 | –0.48 | –0.64 | –0.76 | –0.36 | –0.78 | 0.34 | 0.27 | –0.61 | 0.27 | –0.50 |
| Y | –0.48 | 0.27 | 0.51 | 0.37 | 0.23 | 0.31 | –0.10 | –0.38 | 0.51 | 0.36 | 0.44 |
| Ga | –0.92 | 0.80 | 0.96 | 0.75 | 0.02 | 0.78 | –0.52 | –0.46 | 0.88 | –0.17 | 0.75 |
| La | –0.31 | 0.19 | 0.48 | 0.22 | –0.20 | 0.06 | –0.54 | –0.45 | 0.43 | –0.07 | 0.47 |
| Ce | –0.35 | 0.24 | 0.46 | 0.33 | –0.08 | 0.15 | –0.51 | –0.42 | 0.41 | –0.05 | 0.41 |
| Nd | –0.13 | 0.13 | 0.33 | –0.02 | –0.25 | –0.11 | –0.34 | –0.21 | 0.19 | –0.12 | 0.34 |
| Sm | –0.50 | 0.46 | 0.67 | 0.35 | –0.15 | 0.23 | –0.47 | –0.42 | 0.52 | 0.06 | 0.57 |
| Eu | –0.61 | 0.68 | 0.66 | 0.44 | –0.12 | 0.47 | –0.08 | 0.08 | 0.32 | –0.15 | 0.33 |
| Tb | –0.71 | 0.52 | 0.69 | 0.62 | 0.25 | 0.58 | –0.22 | –0.30 | 0.61 | 0.12 | 0.54 |
| Yb | –0.53 | 0.40 | 0.50 | 0.50 | 0.33 | 0.44 | –0.03 | –0.19 | 0.34 | 0.28 | 0.24 |
| Lu | –0.61 | 0.52 | 0.57 | 0.59 | 0.32 | 0.57 | –0.07 | –0.25 | 0.44 | 0.09 | 0.29 |